Markovian Transparency Control of an Exoskeleton Robot

Felix M. Escalante, Leonardo F. dos Santos, Yecid Moreno, Adriano A. G. Siqueira, Marco H. Terra, and Thiago Boaventura, *Member, IEEE*

***Abstract*—In wearable robotics, certain applications require the robot to be transparent, i.e., imperceptible to the user. This is a very difficult cooperative control task due to the inherent coupling between human and robot, unpredictable human movements, and user-dependent behavior. In this letter, we propose a novel transparency controller based on discrete-time Markovian jump linear systems to minimize the human-robot interaction forces of an exoskeleton robot during walking. Our model-based stochastic control approach describes a gait cycle as an event-dependent Markov chain and uses a given transition matrix to switch between them. An IMU-based Kalman filter is used to perform real-time human state estimation and gait phase detection. The robustness and effectiveness of the proposed controller are demonstrated with experiments on a lower-limb exoskeleton driven by series elastic actuators.**

***Index Terms*—Transparency control, markovian jump linear systems, physical human-robot interaction.**

I. Introduction

In addition to safety, precision, and robustness, comfort is a key requirement for physical Human-Robot Interaction (pHRI) devices, such as exoskeleton robots. In pHRI applications such as physical assistance and power augmentation, to be comfortable often means that the coupled human-robot system must behave similarly to the way humans naturally do. To achieve this, the robot controller should be able to follow the intended human motions with as little delay as possible, minimizing the interaction forces between the human and the robot. This concept is well known in the literature as *transparency control* [1], [2].

Manuscript received 21 June 2022; accepted 3 November 2022. Date of publication 1 December 2022; date of current version 20 December 2022. This letter was recommended for publication by Associate Editor K. Hashtrudi-Zaad and Editor Jee-Hwan Ryu upon evaluation of the reviewers' comments. This work was supported in part by the Coordination for the Improvement of Higher Education Personnel (CAPES) - Finance Code 001, PGPTA, under Grant 3457/2014 and in part by São Paulo Research Foundation (FAPESP) under Grants 2018/15472-9, 2019/05937-7, 2021/09244-6, and 2022/06634-0. *(Corresponding author: Felix M. Escalante.)*

This work involved human subjects or animals in its research. Approval of all ethical and experimental procedures and protocols was granted by Ethics Committee of the University of São Paulo, School of Physical Education and Sport of Ribeirão Preto, EEFER P-USP Application CAAE No. 41150620.7.0000.5659, and performed in line with the decision statement No 4.579.836.

The authors are with the São Carlos School of Engineering, University of São Paulo, São Carlos, SP 13566-590, Brazil (e-mail: maurinho707@usp.br; leonardo.felipe.santos@usp.br; joseyecid18@hotmail.com; siqueira@sc.usp.br; terra@sc.usp.br; tboaventura@usp.br).

This letter has supplementary downloadable material available at https://doi.org/10.1109/LRA.2022.3226034, provided by the authors.

Digital Object Identifier 10.1109/LRA.2022.3226034

In transparency control, the control variable is usually the interaction force and/or torque between the human and the robot, with the desired value, in this case, equal to zero. Different approaches to controlling such interaction forces have been discussed in the literature [2]. Most of them rely on low-gain force or impedance controllers at user interface points [3], [4]. However, fundamental limitations on the stability of such feedback controllers may limit the performance [5]. An option to overcome such stability limitations is to use model-based feedforward controllers to further enhance the performance of transparency controllers [6].

A central question in transparency control is how to obtain the interaction forces signal to be controlled. While some works, e.g. [7], directly measure it, others choose to estimate it [8]. Measuring the interaction force, for example with force/torque sensors at the interaction points, leads to more accurate and instantaneous measurements. However, it is a more expensive solution and often requires substantial modifications to the robot structure and electronics. The interaction force estimation, on the other hand, usually relies on the kinematic and torque measurements already available at the robot joints, and/or on non-invasive sensors, such as Inertial Measurement Units (IMUs), placed on the human body. However, imprecision and drift are issues that usually require additional design and computational efforts to provide reliable results [9], [10]. Other alternative approaches to improve transparency may also include the use of electromyography (EMG) signals [11] and hardware solutions such as clutches [12].

A major challenge in making an exoskeleton robot transparent is handling unexpected and abrupt user movements [13]. To mitigate this issue, we propose a model-based stochastic transparency controller based on discrete-time Markovian Jump Linear Systems (MJLSs). MJSs have been extensively used in the literature for applications that present abrupt changes in dynamic behavior, such as: economic systems [14], power systems [15], communication systems [16], among others stochastic dynamic systems [17]. With this in mind, we define the pHRI as a stochastic discrete-time model of finite transitions subject to a Markovian chain. We previously used EMG signals to define task operation modes in an ankle rehabilitation device [18], [19], as well as Force Sensitive Resistors (FSRs) to detect motion transitions in a knee rehabilitation exoskeleton [20]. Differently, we now propose using IMUs to identify walking gait phases in a full lower limb exoskeleton robot.

In summary, the main contributions of this paper are: 1) a novel stochastic transparency controller based on gait events experimentally validated on a lower-limb exoskeleton using a six-axis force/torque sensor to measure the interaction human-robot forces; 2) a novel Markovian time-variable model of pHRI associated with transitions for a human walking gait phases based on a Markovian chain; and 3) a thorough system modeling that takes into account the dynamics of a Series Elastic Actuator (SEA) exoskeleton, an-IMU based estimation of the human kinematics, as well as a direct measurement of the pHRI forces.

This letter is divided into the following sections. Section II presents the mathematical model of the coupled human-robot system and also the hardware used for experimental analyzes. Section III describes the control method, while Section IV brings the results and related discussions. Finally, some conclusions and future work are provided in Section V.

II. System Modeling, Estimation, and Description

In this section, we model the pHRI using a MJLS approach; present the IMU-based estimator for the human joint states; explain the detection of the phases of a walking gait; and also introduce the exoskeleton hardware.

A. Coupled Human-Robot Dynamics

The coupled system dynamics can be derived from the dynamics of its main subsystems: robot, human, and human-robot attachment, as shown in Fig. 1. At the attachment point, the interaction torque, τ_i, can be defined as:

$$\tau_i = K_a\left(\phi_r - \phi_h\right) + B_a\left(\dot{\phi}_r - \dot{\phi}_h\right) \tag{1}$$

where K_a and B_a are the stiffness and damping of the attachment, while ϕ_r and ϕ_h define the angular position of the robot and human, respectively. Similarly, the torques applied by the human, τ_h, can be modeled by:

$$K_h(\phi_{eq} - \phi_h) - B_h\dot{\phi}_h = \tau_i + \tau_h \tag{2}$$

where K_h and B_h are the stiffness and damping of the human joint, and ϕ_{eq} can be viewed as an equilibrium angle defined by the user motor control.

The torque τ_r applied by the SEA, present at the exoskeleton joints, is defined as:

$$\tau_r = K_s(\phi_w - \phi_r) \tag{3}$$

where K_s is the stiffness of the SEA spring, ϕ_r is the angular position of the robot link, and ϕ_w the angular position of the worm wheel given by $\phi_w = N_r^{-1}\phi_m$, which is associated with the angular position of the motor ϕ_m and the reduction ratio N_r. By applying Newton's second law to the actuator inertia J_ω and the robot link inertia J_r, the following relations are obtained:

$$J_r\ddot{\phi}_r + B_r\dot{\phi}_r = \tau_r - \tau_i \tag{4}$$

$$J_w\ddot{\phi}_w = N_r\tau_m - \tau_r \tag{5}$$

where B_r is the damping of the robot joint. By isolating $\ddot{\phi}_w$ and $\ddot{\phi}_r$ from (5) and (4), combining them with (3), and considering the fact the motor driver low-level velocity controller gives $\tau_m \approx B_w\omega_m$, where ω_m is the motor velocity, we obtain the following dynamics for τ_r:

$$\ddot{\tau}_r + \frac{(J_r + J_w)K_s}{J_wJ_r}\tau_r - \frac{K_s}{J_r}\tau_i = \frac{N_rB_wK_s}{J_w}\omega_m + \frac{B_rK_s}{J_r}\dot{\phi}_r \tag{6}$$

If we derive both (1) and (2), and then combine them with (4), we can get the following additional dynamics:

$$\dot{\tau}_i - \frac{B_a}{B_h}\dot{\tau}_r + \frac{B_a}{Jr}(\tau_i - \tau_r) = -\frac{B_aB_r}{J_r}\dot{\phi}_r + \frac{K_hB_a}{B_h}\left(\dot{\phi}_h - \dot{\phi}_{eq}\right) + K_a(\dot{\phi}_r - \dot{\phi}_h)\,. \tag{7}$$

Lastly, using (4) and the time derivative of (2), it is possible to isolate the human and robot angular accelerations $\ddot{\phi}_h$ and $\ddot{\phi}_r$ to finally complete the required equations to describe the human-robot coupled dynamics in the following discrete state space form, with $n = 0, 1, \ldots$:

$$\begin{aligned}\mathbf{x}_{n+1} &= \mathbf{F}_{\theta_k,n}\,\mathbf{x}_n + \mathbf{B}_{\theta_k,n}\,u_n + \mathbf{B}^d_{\theta_k,n}\boldsymbol{\tau}^d_r + \mathbf{G}_{\theta_k,n}\,w_n,\\ \mathbf{y}_n &= \mathbf{C}\,\mathbf{x}_n + \mathbf{D}\,u_n\end{aligned} \tag{8}$$

where $\mathbf{x}_n = [\dot{\tau}_r\ \tau_r\ \tau_i\ \dot{\phi}_r\ \phi_r\ \dot{\phi}_h\ \phi_h\ e^i_{\tau_r}]^T \in \mathbb{R}^{8\times1}$ is the state vector, being $e^i_{\tau_r} = \int(\tau^d_r - \tau_r)dt$ the integral error of the robot torque, which is introduced to track the desired robot toque profiles, τ^d_r; $u_n \in \mathbb{R}$ is the control input ω_m; $\mathbf{y}_n = [\tau_r\ \tau_i\ \dot{\phi}_r\ \phi_r\ \dot{\phi}_h\ \phi_h]^T \in \mathbb{R}^{6\times1}$ is the measurement vector. In

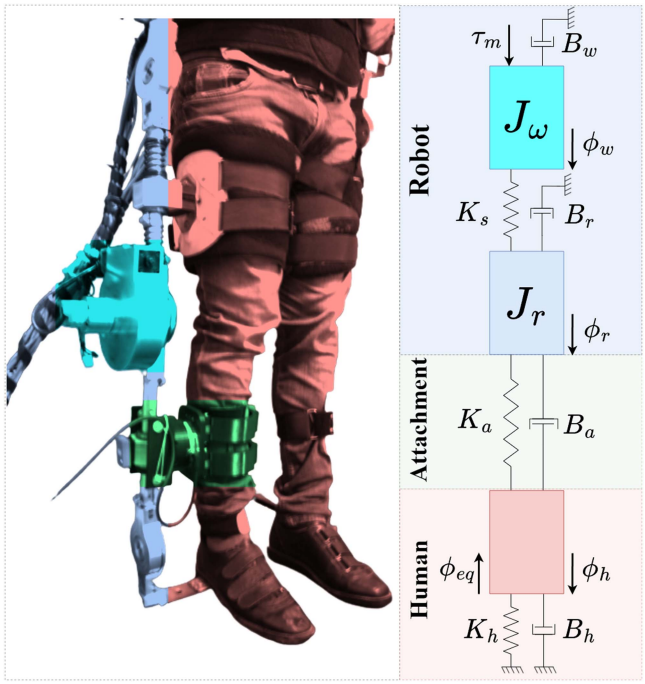

Fig. 1. Representation of the physical system on the left and a schematic block diagram used to model its dynamics on the right. The exoskeleton robot uses SEAs, where the motor torque τ_m accelerates the actuator inertia J_ω, in cyan, and the robot link inertia J_r, in light violet, being K_s the SEA stiffness, B_r and B_ω the viscous friction coefficients of the robot joint and actuator, respectively, and ϕ_r the robot link angular position. The human-robot attachment, in green, is modeled by a spring-damper system with stiffness K_a and damping B_a. Finally, the human, in magenta, is modeled with a damping B_h and a stiffness K_h, a human angular position ϕ_h, and a time-variable human equilibrium angle ϕ_{eq}.

TABLE I
MODEL PARAMETERS, OBTAINED FROM [21] AND [19]

Exoskeleton robot

Parameter	Value	Unit
Exoskeleton's inertia moment J_r	0.885	Kg m^2
Exoskeleton's damping B_r	60	N m s /rad
Exoskeleton's stiffness K_s	105	N m /rad
Motor's inertia moment J_w	0.47	Kg m^2
Motor's damping B_w	0.00287	N m s/ rad
Motor's reduction ratio N_r	150	

Human joint

Parameter	Value	Unit
Knee joint damping by gait phase B_{h,θ_k}	[2 1.2 1.2 4.0 1.5]	N m s /rad
Knee joint stiffness by gait phase K_{h,θ_k}	[175 200 130 400 145]	N m /rad

Attachment point

Parameter	Value	Unit
Attachment damping B_a	10	N m s /rad
Attachment stiffness K_a	200	N m/rad

this approach, we have full access to state information; $w_n \in \mathbb{R}$ is the disturbance vector, composed of $\dot{\phi}_{eq}$; $\mathbf{F}_{\theta_k,n} \in \mathbb{R}^{8\times8}$, $\mathbf{B}_{\theta_k,n} \in \mathbb{R}^{8\times1}$, $\mathbf{B}^d_{\theta_k,n} \in \mathbb{R}^{8\times1}$, $\mathbf{G}_{\theta_k,n} \in \mathbb{R}^{8\times1}$, $\mathbf{C} \in \mathbb{R}^{6\times8}$ and $\mathbf{D} \in \mathbb{R}^{6\times1}$ are nominal parameter matrices and vectors (see Appendix) that depend on the values reported in Table I.

In (8), a jump parameter $\theta_k \in \{1, \ldots, n_M\}$, defines a different coupled system dynamics to each one of the $n_M = 5$ Markovian operation modes used to model the gait cycle, as described in Section II-C.

B. Human Joint State Estimation Based on IMUs

Since we do not instrument the human limbs to obtain the angular position and velocity of the human joints, we need to estimate them. Our strategy to estimate the human kinematic data employs lightweight IMUs strapped on the human limbs. Three sensors are positioned on the leg: on the shank, on the lower leg, and on the heel. The estimated human knee kinematic quantities $\hat{\phi}_h$ and $\dot{\hat{\phi}}_h$ are derived from the shank and lower leg sensor data. The estimated ankle acceleration, $\ddot{\hat{\phi}}_{ak}$, is obtained from the lower leg and the heel sensors.

From [22], a quaternion-based Kalman filter was modified aiming at magnetic disturbance-free estimation. Also, since the joint kinematics quantities of interest are normal to the sagittal plane, the yaw angle ψ was ignored, as it can seen by the quaternion rotation $\hat{\mathbf{x}}(-\psi) \otimes \hat{\mathbf{x}}$ on the Algorithm 1. In this algorithm description, the subscript n represents the discrete-time iteration, while the superscript index j denotes different sensors. Vectors $\mathbf{a}^j$ and $\boldsymbol{\omega}^j$ are the accelerometer and gyroscope data, respectively. The sensor process update is based on an adaptive-step gradient descent with initial step size μ_0, dynamic factor β, and time step T_s. The quaternion error function gradient is $\nabla\mathbf{f}$. Sensor noise matrix is $\mathbf{S}$, process noise matrix is $\mathbf{Q_n}$, estimate uncertainty is $\mathbf{P_n}$, state transition matrix is $\mathbf{G}$ and the observation matrix is $\mathbf{H}$. The state vector is $\mathbf{x_n}$, and the output vector is $\mathbf{z_n}$. The computation of the joint angular velocities considered the rotation matrices defined by the relative quaternions, $\mathbf{R}(\mathbf{q_r})$, mitigating the influence of the IMUs placement on the estimation. This algorithm was evaluated against the off-the-shelf extended Kalman filter (EKF) estimator from the IMUs [23]. Before the human-robot experiments, we

Algorithm 1: Estimator of Human Joint States.

loop :
  for *(j = 0; j < n° IMUs; j++)* **do**
    // Adaptive-Step Gradient Descend:
    $\mu = \mu_0 + \beta T_s |\omega^j|$
    $\mathbf{z^j_n} = \mathbf{x^j_n} - \mu|\nabla\mathbf{f}(\mathbf{x}^j_n, \mathbf{a}^j)|$
    // Kalman - Prediction:
    $\mathbf{\hat{x}^j_n} = \mathbf{G}(\omega^j, T_s)\mathbf{x^j_n}$
    $\mathbf{\hat{P}^j_n} = \mathbf{G}\mathbf{P^j_n}\mathbf{G}^T$
    // Kalman - Update:
    $\mathbf{K_g} = \mathbf{\hat{P}^j_n}\mathbf{H}^T\left[\mathbf{H}\mathbf{\hat{P}^j_n}\mathbf{H}^T + \mathbf{S}\right]^{-1}$
    $\mathbf{\hat{x}^j_{n+1}} = \mathbf{\hat{x}^j_n} + \mathbf{K_g}[\mathbf{z^j_n} - \mathbf{H}\hat{\mathbf{x}}^\mathbf{j}_\mathbf{n}]$
    $\mathbf{\hat{P}^j_{n+1}} = [\mathbf{I} - \mathbf{K_g}\mathbf{H}]\mathbf{\hat{P}^j_n}$
    // Remove Yaw drift:
    $\mathbf{\hat{x}^j_{n+1}} = \mathbf{\hat{x}^j_{n+1}}(-\psi) \otimes \mathbf{\hat{x}^j_{n+1}}$
  end
  for *(j = 0; j < (n° IMUs -1); j++)* **do**
    $\mathbf{q} = \mathbf{\hat{x}^{j+1}_{n+1}} \otimes \mathbf{\hat{x}^j_{n+1}}$
    $\hat{\phi} = atan(2q_0q_1 + 2q_2q_3, q_3^2 + q_0^2 - q_2^2 - q_1^2)$
    $\dot{\hat{\phi}} = \mathbf{R}(\mathbf{q})\omega^{j+1} - \omega^j$
    $\ddot{\hat{\phi}} = (3\dot{\phi}_{n+1} - 4\dot{\phi}_n + \dot{\phi}_{n-1})/(2T_s)$
  end
goto loop

Algorithm 2: Estimation of Walking Gait Subphases.

Define $\theta_k = \{LR, MSt, TSt, ISW, TSW\}$
Define $R_1 \in \mathbb{R} : [1 \leq R_1 \leq 4]$
Define $R_2 \in \mathbb{R} : [1 \leq R_2 \leq 0.4]$
Initialize $\theta_k = LR$
Initialize $\Omega = 0$
loop :
  $\ddot{\hat{\phi}}^n_{ak} \leftarrow$ Value updated from another thread
  switch θ_k **do**
    case LR **:**
      if $\{\ddot{\hat{\phi}}^{(n-1)}_{ak}, \ddot{\hat{\phi}}^n_{ak}\} \in \{-R_1\}$ **and** $(\ddot{\hat{\phi}}^n_{ak} > \ddot{\hat{\phi}}^{(n-1)}_{ak})$ **:** $\theta_k = MSt$
    case MSt **:**
      if $(\ddot{\hat{\phi}}^{(n-1)}_{ak} \leq 0)$ **and** $(\ddot{\hat{\phi}}^n_{ak} \geq 0)$ **:** $\theta_k = TSt$
    case TSt **:**
      if $\{\ddot{\hat{\phi}}^{(n-1)}_{ak}, \ddot{\hat{\phi}}^n_{ak}\} \in \{R_1\}$ **and** $(\ddot{\hat{\phi}}^{(n-1)}_{ak} > \ddot{\hat{\phi}}^n_{ak})$ **:** $\theta_k = ISW$
    case ISW **:**
      if $(\ddot{\hat{\phi}}^{(n-1)}_{ak} \geq 0)$ **and** $(\ddot{\hat{\phi}}^n_{ak} \leq 0)$ **:** $\theta_k = TSW$
    case TSW **:**
      if $\{\ddot{\hat{\phi}}^{(n-1)}_{ak}, \ddot{\hat{\phi}}^n_{ak}\} \in \{-R_2\}$ **:**
        if $(\ddot{\hat{\phi}}^n_{ak} > \ddot{\hat{\phi}}^{(n-1)}_{ak})$ **and** $(\Omega$ **is** $0)$ **:** Ω++
        if $(\ddot{\hat{\phi}}^n_{ak} < \ddot{\hat{\phi}}^{(n-1)}_{ak})$ **and** $(\Omega$ **is** $1)$ **:** Ω++
        if Ω **is** 2 **:** $\Omega = 0$; $\theta_k = LR$
  end
  $\ddot{\hat{\phi}}^{(n-1)}_{ak} \leftarrow \ddot{\hat{\phi}}^n_{ak}$
goto loop

conducted an experimental comparison of our proposed method versus the off-the-shelf EKF. Along 40 seconds, the average angle error was 0.367° on the knee and 1.220° on the ankle. This evaluation was with the user without wearing the robot to avoid magnetic disturbances.

C. Walking Gait Subphases Detection

We split the walking gait cycle into five subphases: loading response (LR), mid-stance (MSt), terminal stance (TSt), initial swing (ISW) and terminal swing (TSW). We then modeled the transitions between these subphases as a Markov chain θ_k using a fourth IMU sensor placed on the human heel based on Algorithm 2. This algorithm has already been tested and validated, with

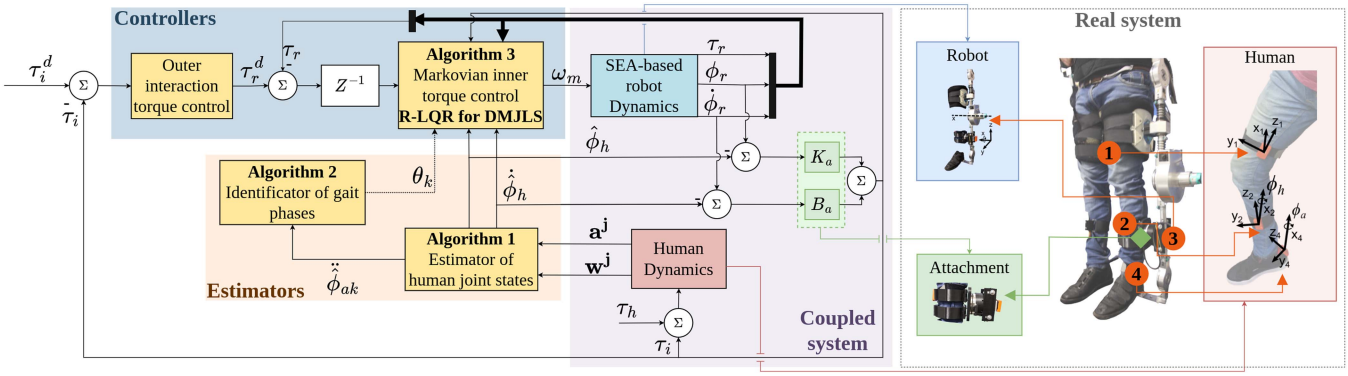

Fig. 2. The transparency control framework is shown on the left, with the respective hardware counterparts on the right.

minor modifications, in patients with hemiparesis, myelopathy, and Parkinson's disease [24], [25]. The algorithm consists of analyzing the estimated ankle angular acceleration $\ddot{\hat{\phi}}_{ak}$ in the sagittal plane. Thresholds R_1 and R_2 are used to classify areas in the gait cycle. Their values depend on the speed of the treadmill and are defined in an initial exercise without the exoskeleton. The variable Ω is used to identify the hell strike event between the TSW and LR subphases. The Algorithm 2 was validated using three Force Sensitive Resistors (FSRs) on the user shoes, located in the heel, toe, and second metatarsus, similarly to [19]. The percentage of correlation was 96.77 % between the estimation with IMU vs. FSR.

The current Markovian operation mode is defined by θ_k, and its transitions by the probability matrix $\mathbb{P} \in \mathbb{R}^{n_M \times n_M}$, being $n_M = 5$ in this case. $\mathbb{P} = [p_{a,b}]$ represents the probability of going from a state to b, satisfying the constraints: $\sum_{b=1}^{n_M} \mathbb{P}_{ab} = 1$ and $0 \leq \mathbb{P}_{ab} \leq 1$,

$$\mathbb{P} = \begin{bmatrix} p_{11} & p_{12} & \cdots & p_{1\,s} \\ p_{21} & p_{22} & \cdots & p_{2\,s} \\ \vdots & \vdots & \ddots & \vdots \\ p_{s1} & p_{s2} & \cdots & p_{ss} \end{bmatrix}. \tag{9}$$

In Markovian systems, future states depend only on current states. Thus, it is possible to define the next operation mode b for $n+1$ from the current Markov state a for n and the transition probabilities without further information on the past Markovian mode. That is,

$$\mathbb{P}_{ab} = \Pr\left(\theta_k^{n+1} = b \,|\, \theta_k^n = a\right). \tag{10}$$

D. Hardware

The experimental platform used in this work was a modular lower-limb exoskeleton, Fig. 2-right, with three joints per leg: two passive (the hip and ankle) and one active (knee). The active knee joint uses a rotary SEA, which consists of a DC motor fixed to a worn gear set with a reduction of $150:1$ and a custom spring with stiffness $K_s = 105$ Nm/rad. The robot torque τ_r is calculated using Hooke's law and the deformation of the spring. To evaluate the performance of the implemented transparency controllers, an ATI Axia80-M50 six-axis force/torque sensor was mounted on the shank attachment, measuring the interaction forces and torques between the user leg and the robot link. The robot control system includes a computer for the real-time control, EPOS 24/5 motor drivers connected with internal velocity control loops based on the PI controllers.

III. Markovian Transparency Control

In this section, we present a transparency controller design based on Markovian theory. The proposed approach consists of a cascade configuration defined by two control loops: a robot torque (τ_r) inner loop shaping the robot dynamics, and an interaction torque (τ_i) outer loop shaping the pHRI, as shown in Fig. 2. The idea behind this configuration is to compensate for the influence of the coupled dynamics, (6)-(7). On the one hand, the inner torque loop must be robust enough to track torque references from the outer interaction torque loop, despite abrupt and sudden changes in human movements. Therefore, the uncertainties of the coupled system in (6) must be corrected for the control signal of the system, the motor velocity ω_m. This is because the SEA-driven exoskeleton operates in a velocity control configuration. On the other hand, the influence of human impedance parameters on the remaining (7) is compensated for by the desired robot torque τ_r^d. Therefore, the outer interaction loop is responsible for modifying the waveform of the robot torque reference to be tracked by the inner torque loop.

A. Inner Markovian Torque Control

The torque control approach is based on the Robust Linear Quadratic Regulator for Discrete-time Markov jump Linear Systems, R-LQR for DMJLS, presented in [26]. Therefore, consider the model (8), which has been rewritten to show the uncertainties of the model as follows:

$$\begin{aligned} \mathbf{x}_{n+1} &= (\mathbf{F}_{\theta_k,n} + \delta\mathbf{F}_{\theta_k,n})\mathbf{x}_n + (\mathbf{B}_{\theta_k,n} + \delta\mathbf{B}_{\theta_k,n})u_n \\ &\quad + \mathbf{B}^d_{\theta_k,n}\boldsymbol{\tau}_r^d + \mathbf{G}_{\theta_k,n}w_n, \\ \mathbf{y}_n &= \mathbf{C}\mathbf{x}_n + \mathbf{D}u_n \end{aligned} \tag{11}$$

where $\delta\mathbf{F}_{\theta_k,n}$, and $\delta\mathbf{B}_{\theta_k,n}$ are uncertain matrices defined as

$$[\delta\mathbf{F}_{\theta_k,n}\ \delta\mathbf{B}_{\theta_k,n}] = \mathbf{H}_{\theta_k,n}\Delta_{\theta_k,n}\left[\mathbf{E}_{F_{\theta_k,n}}\ E_{B_{\theta_k,n}}\right] \tag{12}$$

being $\mathbf{H}_{\theta_k,n} \in \mathbb{R}^{8\times 1}$, $\mathbf{E}_{F_{\theta_k,n}} \in \mathbb{R}^{1\times 8}$, $E_{B_{\theta_k,n}}$ are known matrices, and $\Delta_{\theta_k,n}$ is an arbitrary matrix such that $\| \Delta_{\theta_k,n} \| \leq 1$. The solution to the regulation problem (11) restricted to (12) is achieved by using the Min-Max optimization problem.

$$\min_{\mathbf{x}_{n+1},\mathbf{u}_n} \max_{\delta\mathbf{F}_{\theta_k,n},\delta\mathbf{B}_{\theta_k,n}} \{\, \boldsymbol{\mathcal{J}}_n^{\mu_c}(x_{n+1}, u_n, \delta F_{\theta_k,n}, \delta B_{\theta_k,n})\} \tag{13}$$

where the quadratic functional, $\boldsymbol{\mathcal{J}}_n^{\mu_c}$, is given by:

$$\begin{aligned}\boldsymbol{\mathcal{J}}_n^{\mu_c} = &\begin{bmatrix}\mathbf{x}_{n+1}\\ \mathbf{u}_n\end{bmatrix}^T \begin{bmatrix}\boldsymbol{\Psi}_{\theta_k,n+1} & 0\\ 0 & \boldsymbol{R}_{\theta_k,n}\end{bmatrix}\begin{bmatrix}\mathbf{x}_{n+1}\\ \mathbf{u}_n\end{bmatrix}\\ &+\left\{\begin{bmatrix}\mathbf{0} & \mathbf{0}\\ \mathbf{I} & -\mathbf{B}^{\delta}_{\theta_k,n}\end{bmatrix}\begin{bmatrix}\mathbf{x}_{n+1}\\ \mathbf{u}_n\end{bmatrix}-\begin{bmatrix}-\mathbf{I}\\ \mathbf{F}^{\delta}_{\theta_k,n}\end{bmatrix}\mathbf{x}_n\right\}^T\begin{bmatrix}\mathbf{Q}_{\theta_k,n} & \mathbf{0}\\ \mathbf{0} & \mu_c\mathbf{I}\end{bmatrix}\\ &\left\{\begin{bmatrix}\mathbf{0} & \mathbf{0}\\ \mathbf{I} & -\mathbf{B}^{\delta}_{\theta_k,n}\end{bmatrix}\begin{bmatrix}\mathbf{x}_{n+1}\\ \mathbf{u}_n\end{bmatrix}-\begin{bmatrix}-\mathbf{I}\\ \mathbf{F}^{\delta}_{\theta_k,n}\end{bmatrix}\mathbf{x}_n\right\}\end{aligned} \tag{14}$$

being $\boldsymbol{\Psi}_{\theta_k}(n+1) = \sum_{\theta_k=1}^{5}\mathbf{P}_{\theta_k,n+1}\cdot p_{\theta_{a,b}}$; $\mathbf{P}_{\theta_k,n} > 0$, $\mathbf{Q}_{\theta_k,n} > 0$, and $\mathbf{R}_{\theta_k,n} > 0$ positive definite weighting matrices. The solution to the optimization problem (13) that ensures the optimal state and control sequences for an instant k and a Markov state θ_k is given by the Algorithm 3, where

$$\begin{aligned}\boldsymbol{\mathcal{W}}_{\theta_k,n} &= \begin{bmatrix}\mu_c^{-1}\mathbf{I} - \hat{\lambda}^{-1}_{c,\theta_k,n}\mathbf{H}_{\theta_k,n}\mathbf{H}^T_{\theta_k,n} & 0\\ 0 & \hat{\lambda}^{-1}_{c,\theta_k,n}\mathbf{I}\end{bmatrix},\\ \hat{\mathbf{B}}_{\theta_k,n} &= \begin{bmatrix}\mathbf{B}_{\theta_k,n}\\ E_{B_{\theta_k,n}}\end{bmatrix}\quad \hat{\mathbf{F}}_{\theta_k,n} = \begin{bmatrix}\mathbf{F}_{\theta_k,n}\\ \mathbf{E}_{F_{\theta_k,n}}\end{bmatrix},\\ \hat{\mathbf{I}} &= \begin{bmatrix}\mathbf{I}\\ \mathbf{0}\end{bmatrix},\quad \lambda_{c,\theta_k,n} > \| \mu_c\mathbf{H}^T_{\theta_k,n}\mathbf{H}_{\theta_k,n} \| .\end{aligned} \tag{15}$$

The penalty parameter, $\mu_c > 0$, is responsible for guaranteeing the robustness of the Markovian torque approach. When $\mu_c \to +\infty$, then $\boldsymbol{\mathcal{W}}_{\theta_k,n} \to 0$. As a consequence, the closed-loop response is given by

$$\begin{cases}\mathbf{L}_{\theta_k,n} = \mathbf{F}_{\theta_k,n} + \mathbf{B}_{\theta_k,n}\mathbf{K}_{\theta_k,n}\\ \mathbf{E}_{\mathbf{F}_{\theta_k,n}} + E_{\mathbf{B}_{\theta_k,n}}\mathbf{K}_{\theta_k,n} = \mathbf{0}.\end{cases} \tag{16}$$

B. Outer Interaction Torque Control

To achieve a mechanical transparency property and take advantage of the possibility of measuring the interaction torque τ_i, we define the desired robot torque τ_r^d as follows.

$$\tau_r^d = K_p\left(\tau_i^d - \tau_i\right) + K_d\left(\dot{\tau}_i^d - \dot{\tau}_i\right) \tag{17}$$

where K_p and K_d are, respectively, the proportional and derivative gains to compensate the human impedance parameters of (7). Note that to obtain transparency $\tau_i^d = 0$ and $\dot{\tau}_i^d = 0$. Furthermore, to compensate for the effects of the dynamics of the interaction torque in (7) through the robot torque, $K_p = 1$ and $K_d = \frac{B_h}{B_a}$. Therefore, (17) can be rewritten as

$$\tau_r^d = -\tau_i - \frac{B_h}{B_a}\dot{\tau}_i \tag{18}$$

Algorithm 3: R-LQR for DMJLS.

Define $\theta_k = \{LR, MSt, TSt, ISW, TSW\}$
Define $R_1 \in \mathbb{R} : [1 \leq R_1 \leq 4]$
Define $R_2 \in \mathbb{R} : [1 \leq R_2 \leq 0.4]$
Initialize $\theta_k = LR$
Initialize $\Omega = 0$
loop :
  $\ddot{\phi}^n_{ak} \leftarrow$ Value updated from another thread
  switch θ_k **do**
    case LR **:**
      if $\{\ddot{\phi}^{(n-1)}_{ak}, \ddot{\phi}^n_{ak}\} \in \{-R_1\}$ **and** $(\ddot{\phi}^n_{ak} > \ddot{\phi}^{(n-1)}_{ak})$ **:** $\theta_k = MSt$
    case MSt **:**
      if $(\ddot{\phi}^{(n-1)}_{ak} \leq 0)$ **and** $(\ddot{\phi}^n_{ak} \geq 0)$ **:** $\theta_k = TSt$
    case TSt **:**
      if $\{\ddot{\phi}^{(n-1)}_{ak}, \ddot{\phi}^n_{ak}\} \in \{R_1\}$ **and** $(\ddot{\phi}^{(n-1)}_{ak} > \ddot{\phi}^n_{ak})$ **:** $\theta_k = ISW$
    case ISW **:**
      if $(\ddot{\phi}^{(n-1)}_{ak} \geq 0)$ **and** $(\ddot{\phi}^n_{ak} \leq 0)$ **:** $\theta_k = TSW$
    case TSW **:**
      if $\{\ddot{\phi}^{(n-1)}_{ak}, \ddot{\phi}^n_{ak}\} \in \{-R_2\}$ **:**
        if $(\ddot{\phi}^n_{ak} > \ddot{\phi}^{(n-1)}_{ak})$ **and** $(\Omega$ **is** $0)$ **:** Ω++
        if $(\ddot{\phi}^n_{ak} < \ddot{\phi}^{(n-1)}_{ak})$ **and** $(\Omega$ **is** $1)$ **:** Ω++
        if Ω **is** 2 **:** $\Omega = 0$; $\theta_k = LR$
  end
  $\ddot{\phi}^{(n-1)}_{ak} \leftarrow \ddot{\phi}^n_{ak}$
goto loop

IV. Results and Analyzes

This section presents two experiments to illustrate the robustness of the Markovian transparency control approach to addressing stochastic pHRI problems. Both experiments were approved by the Ethics Committee of the University of São Paulo, School of Physical Education and Sport of Ribeirão Preto, EEFERP-USP, CAAE No. 41150620.7.0000.5659, decision statement Nº 4.579.836.

A. Human Free Movements

The first experiment, which we call *free human movements*, aims to evaluate the transparency of the robot against different human excitations. These excitations are generated by random movements in the sagittal plane without restriction of speed, direction, or force. One of the characteristics adopted in this experiment is the jump parameter θ_k, considered random and not sequential as during a walking gait pattern, for instance. Each element in the matrix rows of (9) has the same value, $p_{a,b} = 0.2$, meaning that the probability of jumping to a given mode is the same for all the 5 Markovian modes.

We recorded, for the five Markovian modes, the average interaction torque τ_i and the misalignment of the coupled system $\Delta\phi = \phi_r - \phi_h$. Fig. 3 shows the response of the Markovian interaction controller during the experiment. The average interaction torque was -0.44 ± 2.5 Nm. This value is comparable to other transparency control methods in the literature, such as

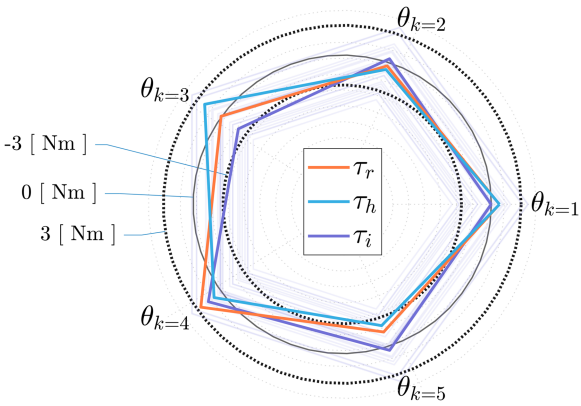

Fig. 3. Average values for τ_i, τ_r, and τ_h. Light purple lines indicate the interaction torque along each jump into the Markov chain, and solid black line indicates the desired interaction torque, $\tau_i^d = 0$.

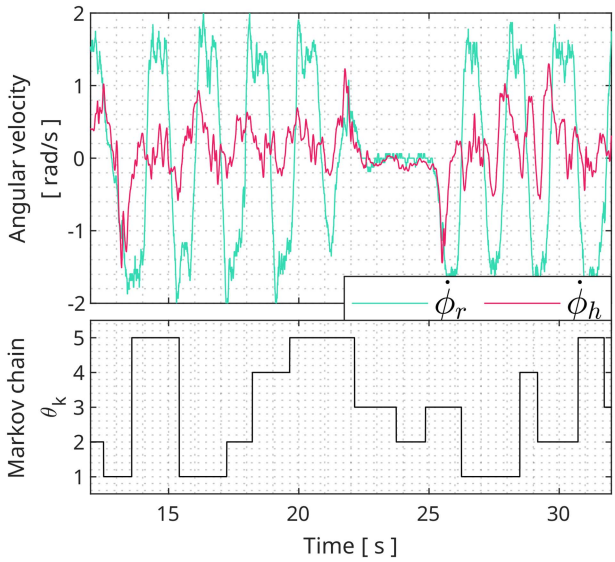

Fig. 4. Temporal response of angular velocities on the top and the Markov chain on the bottom for the human free movement experiment.

in [27], where the mean pHRI torques were reported around 0.5 Nm, at the joint speed 1.57 rad/s. The paper in [28] assessed the transparency under static loads: the interaction reported was about 0.3 Nm with a payload of 4.5 kg.

In this experiment, the randomness of the *free* motions performed by the human subject aimed to introduce sudden and abrupt changes in HRI dynamics, which are also characteristics of people with gait disorders, where the gait does not follow the natural pattern. Therefore, although we did not perform experiments with people with disabilities, the results obtained with these tests demonstrate the potential of our transparency method to deal with such users.

Regarding the misalignment between the robot and human joints, the maximum value obtained during the experiments was 0.12 ± 0.13 rad. This low value is likely caused by the robot's ability to follow user movements despite the weight of the robot, and even sudden and abrupt changes in user speed and direction, Fig. 4. However, the user had greater ease performing

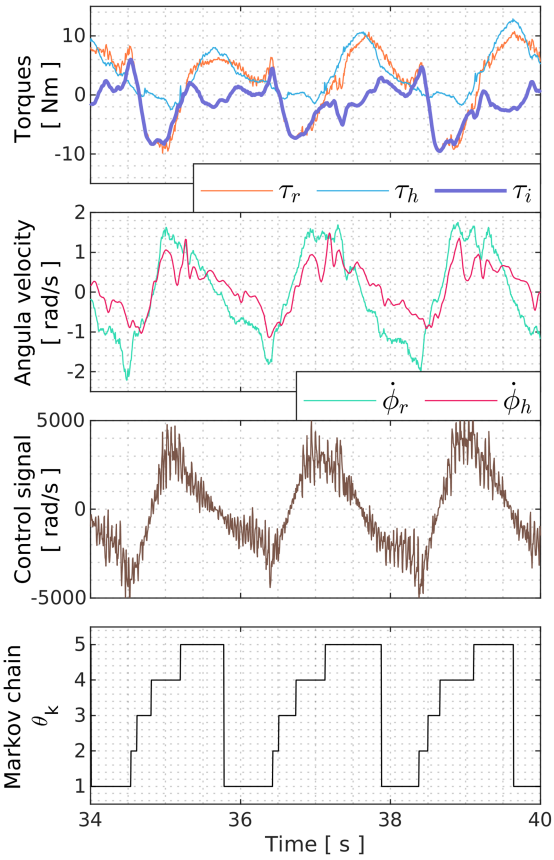

Fig. 5. Human-exoskeleton interaction throughout gait. The graphs illustrate (top) torques; (top-middle) velocities; (bottom-middle) the control signal; and (bottom) Markov chain (black).

the movement with less effort using the Markovian strategy. The maximum human knee angular velocity was 1.15 rad/s.[1] These results should be interpreted with caution, as one of the five operating modes showed undesirable variance, that is, $\tau_i \approx 0$ when $\theta_k = 1, 2, 4, 5$ and $\tau_i \approx -0.15 \pm 4.8\ Nm$ when $\theta_k = 3$.

B. Human-Exoskeleton Interaction Throughout the Gait

The second experiment is called *human-exoskeleton interaction throughout the gait*. Here, a treadmill walking at constant speed (2 km/h) was performed. In this scenario, collisions resulting from foot touch-down events increase the difficulty of ensuring the stability and performance of the controller. Because of this, we defined that the probability that the system remains in the current state is high, and thus we adopted $p_{a,a} = 0.9$. This implies that the probability of jumping to the imminent next state must be $p_{a,b} = 0.1$.

Fig. 5 shows the temporal response of the Markovian transparency control for 1 minute of the experiment.[2] We can observe how the controller remained stable with comparable performance in four of five gait phases despite collisions with the ground and the human-dynamics transitions. As noted in a

[1]For more details on this experiment, see the video https://youtu.be/KGh-DtkUoqE?t=10

[2]See the video for more details https://youtu.be/KGh-DtkUoqE?t=70

TABLE II
STATISTICAL ANALYSIS. THE DATA CONTAIN THE MEAN VALUES OF THE INTERACTION TORQUE AND MISALIGNMENT

	PID		Markovian	
θ_k	$\Delta\phi$ [rad]	τ_i [Nm]	$\Delta\phi$ [rad]	τ_i [Nm]
1	-0.29 ± 0.07	-0.70 ± 1.30	-0.02 ± 0.05	-1.0 ± 0.90
2	-0.26 ± 0.12	4.21 ± 0.85	-0.16 ± 0.03	-0.26 ± 1.16
3	-0.27 ± 0.06	-0.83 ± 3.50	-0.05 ± 0.15	-4.38 ± 1.20
4	-0.07 ± 0.08	-1.41 ± 1.3	0.13 ± 0.06	0.15 ± 0.75
5	-0.3 ± 0.02	0.46 ± 0.12	0.11 ± 0.01	-0.15 ± 0.25

previous experiment, in the case of the TSt phase, $\theta_k = 3$, the behavior of the interaction torque did not match expectations, with an absolute value of up to 7 Nm.

There might be various reasons for the controller performance to decrease in this specific phase. We rule out that this may be due to constant impacts of the foot on the ground, because in the previous experiment, the foot was off and the control system was already compromising its performance.

To better assess the performance of the Markovian transparency controller, we also designed a standard PID-based transparency controller to compare the performance of the controllers in terms of interaction torque τ_i and misalignment $\Delta\phi$. This new analysis is performed by segmenting each stride for one minute into gait subphases separated by events. Table II reports the average values of the interaction torque and the misalignment segmented by phase. For the PID controller, four of the five gait phases were misaligned and τ_i was affected when the system reached maximum misalignment peaks during the experiment. Moreover, the average misalignment was higher for the PID than for the Markovian controller.

V. CONCLUSION

In this letter, we presented a Markovian modeling and control approach to provide transparency in human-exoskeleton motions. Our approach aimed to attenuate stochastic disturbances of human dynamics through a cascade control configuration. As the proposed controller needed kinematic information from the user and current motion phase, we developed IMU-based estimators that performed satisfactorily. To assess the controller performance and stability, we performed two different experiments: one considering situations with high uncertainty, where the user was free to move as they wish, as well as more predictable situations with movement patterns determined by a walking gait cycle. These motions were modeled by a Markov chain that splits the motion into five subphases. The experimental results showed that the developed framework is stable, robust, and safe. Compared to a traditional PID controller, the Markovian controller showed better performance. Future work includes implementing a feedforward inverse dynamics control as well as an interaction force estimator, which would allow to remove the dependency of force sensors measurements. Furthermore, a detailed comparative study of control strategies is needed focusing on protocols that involve more individuals.

APPENDIX

The matrices $\mathbf{F}_{\theta_k,n}$, $\mathbf{B}_{\theta_k,n}$, $\mathbf{B}^d_{\theta_k,n}$, $\mathbf{G}_{\theta_k,n}$, $\mathbf{C}$, and $\mathbf{D}$ that describe the coupled human-robot dynamics for the Markovian operation modes are defined as:

$$\mathbf{F}_{\theta_k,n} = \begin{bmatrix} \mathbf{I} + \mathbf{F}T_s\rho & \mathbf{0} \\ \mathbf{C_F} & 1 \end{bmatrix}, \tag{19}$$

where

$$\mathbf{F} = \begin{bmatrix} 0 & F_{12} & F_{13} & F_{14} & 0 & 0 & 0 \\ 1 & 0 & 0 & 0 & 0 & 0 & 0 \\ F_{31} & F_{32} & F_{33} & F_{34} & 0 & F_{36} & 0 \\ 0 & F_{42} & F_{43} & F_{44} & 0 & 0 & 0 \\ 0 & 0 & 0 & 1 & 0 & 0 & 0 \\ F_{61} & 0 & 0 & 0 & 0 & F_{66} & 0 \\ 0 & 0 & 0 & 0 & 0 & 1 & 0 \end{bmatrix},$$

with

$$F_{12} = -\frac{K_s(J_r + J_w)}{J_w \cdot J_r}; \quad F_{13} = \frac{K_s}{J_r}; \quad F_{14} = \frac{K_s \cdot B_r}{J_r};$$

$$F_{31} = \frac{1}{B_{h,\theta_k}}; \quad F_{32} = \frac{1}{J_r}; \quad F_{33} = -\frac{B_a}{J_r};$$

$$F_{34} = \frac{(J_r \cdot K_a) - (B_a \cdot B_r)}{J_r};$$

$$F_{36} = \frac{(K_{h,\theta_k} \cdot B_a) - (K_a \cdot B_{h,\theta_k})}{B_{h,\theta_k}}; \quad F_{42} = \frac{1}{J_r};$$

$$F_{43} = -\frac{1}{J_r}; \quad F_{44} = -\frac{1}{J_r}; \quad F_{61} = -\frac{1}{B_{h,\theta_k}};$$

$$F_{66} = -\frac{K_{h,\theta_k}}{B_{h,\theta_k}}.$$

$$\mathbf{C_F} = \begin{bmatrix} 0 & -T_s & 0 & 0 & 0 & 0 & 0 \end{bmatrix}; \quad \rho = \sum_{\alpha=0}^{10} \frac{\mathbf{F}^\alpha \cdot T_s^\alpha}{(s+1)!}.$$

$$\mathbf{B}_{\theta_k,n} = \begin{bmatrix} \rho T_s \mathbf{B} \\ 0 \end{bmatrix}, \tag{20}$$

where

$$\mathbf{B} = \begin{bmatrix} B_{11} & 0 & 0 & 0 & 0 & 0 & 0 \end{bmatrix}^T,$$

with

$$B_{11} = \frac{K_s \cdot N_r \cdot B_w}{J_w}.$$

$$\mathbf{B}^d_{\theta_k,n} = \begin{bmatrix} \mathbf{0} \\ T_s \end{bmatrix}, \tag{21}$$

$$\mathbf{G}_{\theta_k,n} = \begin{bmatrix} \rho T_s \mathbf{G} \\ 0 \end{bmatrix}, \tag{22}$$

where

$$\mathbf{G} = \begin{bmatrix} 0 & 0 & G_{31} & 0 & 0 & G_{61} & 0 \end{bmatrix}^T,$$

with

$$G_{31} = -\frac{B_a \cdot K_{h,\theta_k}}{B_{h,\theta_k}}; \quad G_{61} = \frac{K_{h,\theta_k}}{B_{h,\theta_k}}.$$

$$\mathbf{C} = \begin{bmatrix} 0 & 1 & 0 & 0 & 0 & 0 & 0 & 0 \\ 0 & 0 & 1 & 0 & 0 & 0 & 0 & 0 \\ 0 & 0 & 0 & 1 & 0 & 0 & 0 & 0 \\ 0 & 0 & 0 & 0 & 1 & 0 & 0 & 0 \\ 0 & 0 & 0 & 0 & 0 & 1 & 0 & 0 \\ 0 & 0 & 0 & 0 & 0 & 0 & 1 & 0 \end{bmatrix}, \tag{23}$$

and

$$\mathbf{D} = \begin{bmatrix} 0.01 & 0.1 & 0 & 0.01 & 0 & 0.01 \end{bmatrix}^T. \tag{24}$$

Finally, $\mathbf{I} \in \mathbb{R}^{7\times 7}$, $\mathbf{0} \in \mathbb{R}^{7\times 1}$, and $T_s = 0.005$ s is the sampling time. The parameters for the human and exoskeleton used to obtain the above space-state model are defined in Table I.

REFERENCES

[1] N. Jarrassé, J. Paik, V. Pasqui, and G. Morel, "Experimental evaluation of several strategies for human motion based transparency control," in *Experimental Robotics*. O. Khatib, V. Kumar, and G. J. Pappas, Eds., Berlin, Heidelberg: Springer, 2009, pp. 557–565.

[2] V. Alonso and P. D. L. Puente, "System transparency in shared autonomy: A mini review," *Front. Neurorobot.*, vol. 12, no. 83, pp. 1–11, 2018.

[3] A. Calanca, R. Muradore, and P. Fiorini, "A review of algorithms for compliant control of stiff and fixed-compliance robots," *IEEE/ASME Trans. Mechatronics*, vol. 21, no. 2, pp. 613–624, Apr. 2016.

[4] W. Roozing, J. Malzahn, N. Kashiri, D. G. Caldwell, and N. G. Tsagarakis, "On the stiffness selection for torque-controlled series-elastic actuators," *IEEE Robot. Automat. Lett.*, vol. 2, no. 4, pp. 2255–2262, Oct. 2017.

[5] E. Colgate and N. Hogan, "The interaction of robots with passive environments: Application to force feedback control," in *Proc. Adv. Robot.*, 1989, pp. 465–474.

[6] T. Boaventura and J. Buchli, "Acceleration-based transparency control framework for wearable robots," in *Proc. IEEE/RSJ Int. Conf. Intell. Robots Syst.*, 2016, pp. 5683–5688.

[7] Y. Zimmermann, A. Forino, R. Riener, and M. Hutter, "ANYexo: A versatile and dynamic upper-limb rehabilitation robot," *IEEE Robot. Automat. Lett.*, vol. 4, no. 4, pp. 3649–3656, Oct. 2019.

[8] T. Boaventura, L. Hammer, and J. Buchli, "Interaction force estimation for transparency control on wearable robots using a Kalman filter," in *Proc. Converging Clin. Eng. Res. Neurorehabilitation II*, 2017, pp. 489–493.

[9] K. Haninger, A. Asignacion, and S. Oh, "Safe high impedance control of a series-elastic actuator with a disturbance observer," in *Proc. IEEE Int. Conf. Robot. Automat.*, 2020, pp. 921–927.

[10] A. Asignacion, K. Haninger, S. Oh, and H. Lee, "High-stiffness control of series elastic actuators using a noise reduction disturbance observer," *IEEE Trans. Ind. Electron.*, vol. 69, no. 8, pp. 8212–8219, Aug. 2022.

[11] X. Chen, Y. Zeng, and Y. Yin, "Improving the transparency of an exoskeleton knee joint based on the understanding of motor intent using energy kernel method of EMG," *IEEE Trans. Neural Syst. Rehabil. Eng.*, vol. 25, no. 6, pp. 577–588, Jun. 2017.

[12] T. Zhang and H. Huang, "Design and control of a series elastic actuator with clutch for hip exoskeleton for precise assistive magnitude and timing control and improved mechanical safety," *IEEE/ASME Trans. Mechatronics*, vol. 24, no. 5, pp. 2215–2226, Oct. 2019.

[13] B. Zhong, K. Guo, H. Yu, and M. Zhang, "Toward gait symmetry enhancement via a cable-driven exoskeleton powered by series elastic actuators," *IEEE Robot. Automat. Lett.*, vol. 7, no. 2, pp. 786–793, Apr. 2022.

[14] G. Ma, C. C. Siu, S.-P. Zhu, and R. J. Elliott, "Optimal portfolio execution problem with stochastic price impact," *Automatica*, vol. 112, no. 108739, pp. 1–11, 2020.

[15] H. Soliman and M. Shafiq, "Robust stabilisation of power systems with random abrupt changes," *IET Gener., Transmiss. Distrib.*, vol. 9, no. 15, pp. 2159–2166, 2015.

[16] Y. Zhu, Z. Zhong, W. X. Zheng, and D. Zhou, "HMM-based $\mathcal{H}_\infty$ filtering for discrete-time Markov jump LPV systems over unreliable communication channels," *IEEE Trans. Syst., Man, Cybern. Syst.*, vol. 48, no. 12, pp. 2035–2046, Dec. 2018.

[17] B. Zheng, Q. Xuan, and C. Li, "A minimalistic stochastic dynamics model of cluttered obstacle traversal," *IEEE Robot. Automat. Lett.*, vol. 7, no. 2, pp. 5119–5126, Apr. 2022.

[18] F. M. Escalante, A. L. Jutinico, J. C. Jaimes, A. A. G. Siqueira, and M. H. Terra, "Robust Kalman filter and robust regulator for discrete-time Markovian jump linear systems: Control of series elastic actuators," in *Proc. IEEE Conf. Control Technol. Appl.*, Copenhagen, Denmark, 2018, pp. 976–981.

[19] F. M. Escalante, J. C. Pérez-Ibarra, J. C. Jaimes, A. A. Siqueira, and M. H. Terra, "Robust Markovian impedance control applied to a modular knee-exoskeleton," *IFAC-PapersOnLine*, vol. 53, no. 2, pp. 10141–10147, Jul. 2020.

[20] F. M. Escalante, A. L. Jutinico, J. C. Jaimes, M. H. Terra, and A. A. G. Siqueira, "Markovian robust filtering and control applied to rehabilitation robotics," *IEEE/ASME Trans. Mechatronics*, vol. 26, no. 1, pp. 491–502, Feb. 2021.

[21] W. M. dos Santos, G. A. Caurin, and A. A. Siqueira, "Design and control of an active knee orthosis driven by a rotary series elastic actuator," *Control Eng. Pract.*, vol. 58, pp. 307–318, 2017.

[22] L. Wang, Z. Zhang, and P. Sun, "Quaternion-based Kalman filter for AHRS using an adaptive-step gradient descent algorithm," *Int. J. Adv. Robot. Syst.*, vol. 12, no. 9, 2015, Art. no. 131.

[23] H. Loose and K. Orlowski, "Gait patterns in standard scenarios: Using xsens MTW inertial measurement units," in *Proc. 16th Int. Conf. Res. Educ. Mechatronics*, 2015, pp. 296–300.

[24] J. C. Pérez-Ibarra, A. A. G. Siqueira, and H. I. Krebs, "Real-time identification of gait events in impaired subjects using a single-IMU foot-mounted device," *IEEE Sensors J.*, vol. 20, no. 5, pp. 2616–2624, Mar. 2020.

[25] J. C. Pérez-Ibarra, A. A. G. Siqueira, and H. I. Krebs, "Identification of gait events in healthy and Parkinson's disease subjects using inertial sensors: A supervised learning approach," *IEEE Sensors J.*, vol. 20, no. 24, pp. 14984–14993, Dec. 2020.

[26] J. P. Cerri and M. H. Terra, "Recursive robust regulator for discrete-time Markovian jump linear systems," *IEEE Trans. Autom. Control*, vol. 62, no. 11, pp. 6004–6011, Nov. 2017.

[27] F. Just et al., "Exoskeleton transparency: Feed-forward compensation VS. disturbance observer," *at-Automatisierungstechnik*, vol. 66, no. 12, pp. 1014–1026, 2018.

[28] H. J. Asl, K. Katagiri, T. Narikiyo, M. Yamashita, and M. Kawanishi, "Augmenting human power by assistive robots: Application of adaptive neural networks," *Control Eng. Pract.*, vol. 110, 2021, Art. no. 104769.